Meson Spectra from a Dynamical Three-Field Model of AdS/QCD

A THESIS
SUBMITTED TO THE FACULTY OF THE GRADUATE SCHOOL
OF THE UNIVERSITY OF MINNESOTA
BY

Sean Peter Bartz

IN PARTIAL FULFILLMENT OF THE REQUIREMENTS
FOR THE DEGREE OF
DOCTOR OF PHILOSOPHY

Joseph I. Kapusta

August, 2014

Acknowledgements

There are many people that have earned my gratitude for their contribution to my time in graduate school.

Dedication

To my parents, Larry and Colleen, my first teachers. To my sister, Haley, my first student. To my wife, Alicia, my greatest support.

Abstract

Gauge/gravity dualities are a tool that allow the analytic analysis of strongly-coupled gauge theories. The Anti-de Sitter Space/Conformal Field Theory conjecture posits a duality between ten-dimensional string theory and a super Yang-Mills theory. A phenomenologically-motivated modification of this correspondence is known as AdS/QCD, a duality between strongly-coupled QCD-like theories and weakly-coupled gravitational theories in an additional dimension. QCD is not scale-invariant, so the dual theory must be modified in the conformal dimension to reflect this.

This thesis examines "soft-wall" models of AdS/QCD, wherein the conformal symmetry is broken by a field known as a dilaton. The dynamics of the dilaton and other background fields are examined, and a potential for these fields is determined. The background fields are numerically derived from this potential and used in the calculation of meson spectra, which match well to experiment.

The work presented here is based upon previously-published work by the author:

Contents

List of Tables

List of Figures

Chapter 1

Introduction

- Chapter 2 briefly presents the history of, and science behind, the subjects presented in this thesis.

- In Chapter 3 the experiment is outlined.

- Chapter 4 describes the simulation process used in the analysis.

- Chapter 5 follows the chain of reconstruction software used to obtain meaningful results from data.

- Chapter 6 hashes out the strategy for analysis and presents the data and simulated sets that will be used in the analysis.

- Chapter 7 demonstrates the implementation of the event selection processes.

- In Chapter 8 those events selected in Chapter 7 are analyzed.

- Chapter 9 presents a final discussion of the analyses presented in the thesis.

Chapter 2

Soft-Wall Model

The four-dimensional fields of QCD live in the five-dimensional anti-de Sitter space, with a metric given by

$$ds^2 = a^2(z)(\eta_{\mu\nu}dx^\mu dx^\nu + dz^2), \qquad z \geq 0, \tag{2.1}$$

where $a(z) = L/z$ is the warp factor and L is the AdS curvature radius.

The bulk coordinate z is associated with inverse energy scales, with the ultraviolet limit of QCD represented by fields at $z \to 0$[?]. The AdS/CFT dictionary [?, ?] states that each operator $\mathcal{O}(x)$ in the 4D conformal field theory is associated with a bulk field $\psi(x, z)$. The values of the bulk fields at the UV boundary act as sources for the corresponding 4D currents. Global symmetries of the 4D field theory become gauged symmetries for the bulk fields.

The field content of the 5D theory is dictated by the operators relevant to the chiral dynamics of QCD. The gauge fields $A_{L\,\mu}$, $A_{R\,\mu}$ correspond to the left- and right-handed currents of the $SU(N_f)_L \times SU(N_f)_R$ chiral symmetry, where N_f is the number of quark flavors in the model. The scalar field X is associated with the chiral operator $\bar{q}q$ [?]. The masses of the bulk fields are set by the AdS/CFT relation [?] $m_5^2 L^2 = (\Delta - p)(\Delta + p - 4)$, where Δ is the dimensionof the p-form QCD operator. Table 2.1 illustrates the fields and operators of our model, showing that the scalar field is the only field in this model that is not massless.

The simplest soft-wall action involving the fields from Table 2.1 is given in [?] as

4D Operator	5D Field	p	Δ	$m_5^2 L^2$
$\bar{q}_L \gamma^\mu t^a q_L$	$A_{L\,\mu}^a$	1	3	0
$\bar{q}_R \gamma^\mu t^a q_R$	$A_{R\,\mu}^a$	1	3	0
$\bar{q}_R^\alpha q_L^\beta$	$\frac{2}{z} X^{\alpha\beta}$	0	3	-3

Table 2.1: Operators and fields of the model. The matrices t^a are the generators of the $SU(N_f)$ symmetry.

$$S_5 = \int d^5 x \sqrt{-g}\, e^{-\phi(z)} Tr\left[|DX|^2 + m_X^2 |X|^2 + \frac{1}{4g_5^2}(F_L^2 + F_R^2) \right]. \tag{2.2}$$

The 5D gauge coupling constant g_5 is fixed by calculating the vector current two-point function using this model and then comparing this to the leading order result from QCD, leading to the identification $g_5^2 = 12\pi^2/N_c$ [?]. The field X includes both the scalar and pseudoscalar fields in a representation that will be discussed in Section 2.2.1. The field strength tensors and covariant derivative are defined as

$$F_{L,R}^{MN} = \partial^M A_{L,R}^N - \partial^N A_{L,R}^M - i[A_{L,R}^M, A_{L,R}^N]$$

$$D^M X = \partial^M X - iA_L^M X + iX A_R^M.$$

To describe the vector and axial-vector mesons, we define the fields $V^M = \frac{1}{2}(A_L^M + A_R^M)$ and $A^M = \frac{1}{2}(A_L^M - A_R^M)$. It is convenient to write the action in terms of the fields that describe physical particles with the following re-definitions

$$(F_A^2 + F_V^2) = 2(F_L^2 + F_R^2) \tag{2.3}$$

$$D_M X = \partial_M X - i\{A_M^a, X\} + i[V_M^a, X] \tag{2.4}$$

The scalar field X takes on a z-dependent vacuum expectation value (VEV), breaking the chiral symmetry. In a flavor-symmetric model, the VEV has the form $X_0 = \langle X \rangle = \frac{v(z)}{2} I$, where I is the $N_f \times N_f$ identity matrix. From the AdS/CFT dictionary established in [?, ?], $v(z)$ has the ultraviolet asymptotic form

$$\lim_{z \to 0} v(z) = m_q z + \sigma z^3, \tag{2.5}$$

where m_q is the quark mass and $\sigma = \langle \bar{q}q \rangle$ is the chiral condensate, the variation of the vacuum energy with respect to m_q. In [?], it is shown that, when $v(z)$ is defined by (2.5) over the whole range of z, the chiral condensate is proportional to the quark mass. Thus, the spontaneous and explicit chiral symmetry breaking terms are related, contrary to expectations.

As an example calculation, we can derive the mass spectrum of the vector ρ mesons by varying the vector field and using the axial gauge condition $V_z = 0$. We can separate out the $z-$dependence of the field: $V_\mu^n = \mathcal{V}_\mu^n(x)V_n(z)$, where $V_n(z)$ are the Kaluza-Klein modes. The equation of motion is now one dimensional

$$-\partial_z^2 V_n + \omega' \partial_z V_n = m_{V_n}^2 V_n \tag{2.6}$$

where $\omega = \phi(z) + \log z$, and $(')$ represents differentiation with respect to z, unless otherwise noted. We can eliminate the first derivative of the field, bringing the equation of motion into Schrodinger-like form, using the substitution $V_n(z) = e^{\omega/2}v_n(z)$. The equation of motion is now

$$-v_n'' + \left(\frac{1}{4}\omega'^2 - \frac{1}{2}\omega'' \right) v_n = m_{V_n}^2 v_n. \tag{2.7}$$

This is the general method for finding the equations of motion for the various fields. Using the asymptotic form of the dilaton $\phi = \lambda z^2$, the mass eigenvalues can be found exactly for this model. The equation of motion is now

$$-v_n'' + \left(\lambda z^2 + \frac{3}{4z^2} \right) v_n = m_n^2 v_n. \tag{2.8}$$

The eigenvalues for this equation are $m_n^2 = \lambda(4n+4)$ for $n = 0, 1, 2, 3, \ldots$ The parameter λ is set by matching this trajectory to experimental data. The equation of motion for the axial sector is derived using the same method, yielding

$$-a_n'' + \left(\frac{1}{4}\omega'^2 - \frac{1}{2}\omega'' + g_5^2 \frac{L^2}{z^2} v^2(z) \right) a_n = m_{V_n}^2 a_n. \tag{2.9}$$

The only difference from (2.7) is the presence of the z-dependent mass term involving the VEV. The significant drawbacks for this simple soft-wall model are the relatively poor modeling of the ground state and lower resonances and the lack of independent spontaneous and explicit chiral symmetry breaking terms.

2.1 Modified Soft-Wall Model

An improvement on the soft-wall model, suggested in [**?**], is adding higher-order terms of X to the scalar potential, separating the spontaneous and explicit chiral symmetry breaking. The model established in [**?**] adds a quartic scalar term to the action:

$$S_5 = \int d^5x \sqrt{-g}\, e^{-\phi(z)} Tr\left[|DX|^2 + m_X^2 |X|^2 - \kappa |X|^4 + \frac{1}{2g_5^2}(F_A^2 + F_V^2)\right], \qquad (2.10)$$

where κ is a parameter to be fit to the data. Taking $X = X_0$ and varying (2.10), we find that $v(z)$ has the following nonlinear equation of motion:

$$\partial_z(a^3 e^{-\phi} \partial_z v(z)) - a^5 e^{-\phi}\left(m_X^2 v(z) - \frac{\kappa}{2} v^3(z)\right) = 0. \qquad (2.11)$$

The VEV retains the same UV asymptotic form (2.5), while the non-restoration of chiral symmetry dictates that $v(z) \sim z$ in the infrared region. The VEV is parameterized so that it matches the expected asymptotic behavior. A suitable form was found and justified in [**?**]

$$v(z) = \alpha z + \beta \tanh(\gamma z^2) \qquad (2.12)$$

with the parameters defined as follows

$$\alpha = \frac{\sqrt{3} m_q}{g_5 L}, \qquad \beta = \sqrt{\frac{4\lambda}{\kappa L^2}} - \alpha, \qquad \gamma = \frac{g_5 \sigma}{\sqrt{3}\beta}.$$

The quark mass and chiral condensate can each be taken to zero independently, and the non-restoration of chiral symmetry does not depend on eitherof these parameters. Thus, the spontaneous and chiral symmetry breaking occur separately, as desired. Using (2.12) in (2.11) we can solve for the dilaton field.

Equations of motion are then derived using the method of Section 2, and the equations of motion for the vector and axial fields have thesame form as 2.7 and (2.9), respectively. Due to the more complicated forms for v and ϕ, the eigenvalues are not analytically solvable, so a numerical shooting method is used to calculate the mass spectra for the scalar, vector, and axial sectors. The results for the vector mesons are shown in Figure **??**, and the scalar and axial sectors show similarly good results [**?**]. These results reproduce the linear trajectories found in the simple soft-wall model [**?**] for large n, while improving the agreement of the lower excitations with data.

2.2   Pions in Soft-Wall AdS/QCD

The mass spectrum for the pseudoscalar mesons was not found in the original paper [**?**] because the equations of motion are coupled, second order differential equations, and because of some subtleties that arise when considering the representation of the pseudoscalar field. The paper [**?**] attempted to circumvent these problems by reducing the equations of motion to a single second-order equation, solvable by the shooting method, but their results seemed to miss certain essential features of the pion spectrum. The authors later address this apparent discrepancy in [**?**]. This modified soft-wall model was later completed in the paper [**?**], which clarified the discrepancies between two common representations of the pseudoscalar field, calculated the pion mass spectrum to good accuracy, and derived the Gell-Mann–Oakes–Renner relation from the model.

2.2.1   Pseudoscalar Representation

As mentioned above, the field X contains both the field representing the scalar mesons, S, and the field representing the pseudoscalars, π, as well as the VEV. There are two common ways to represent this field:

$$X_e \;=\; \left(\frac{v(z)}{2} + S(x,z) \right) I e^{2i\pi_e(x,z)^a t^a} \tag{2.13}$$

$$X_l \;=\; \left(\frac{v(z)}{2} + S(x,z) \right) I + i\pi_l(x,z)^a t^a \tag{2.14}$$

with I the $N_f \times N_f$ identity matrix and t^a the $SU(N_f)$ generators. We will refer to X_e as the exponential representation and X_l as the linear representation. Apparent differences between the representations arise as we note that π_e and π_l have different dimensionality. In addition, the linear representation has a quartic interaction term in the Lagrangian, in contrast to the exponential representation. Equations of motion derived from each representation are shown to be equivalent.

Exponential Representation

Let us take (2.14) and substitute it into (2.10), keeping terms that include the field $\pi(\mathbf{x}, z)$, as well as terms that will mix with π,

$$\mathcal{L}_e \;=\; -\sqrt{-g}\,\mathrm{e}^{-\chi(z)} \frac{1}{2} \delta^{ab} \Big(g^{MN} (v^2\, \partial_M \pi \partial_N \pi + v^2 A_M A_N - 2v^2 \partial_M \pi A_N)$$

$$+\frac{g^{MP}g^{NR}}{g_5^2}(\partial_M A_N \partial_P A_R - \partial_M A_N \partial_R A_P)\Big) + \dots \tag{2.15}$$

We work in the axial gauge, $A_z = 0$, and separate A_μ into its transverse and longitudinal components: $A_\mu = A_{\mu\perp} + \partial_\mu\varphi$, where $\partial_\mu A_\perp^\mu = 0$. Separating (2.15) explicitly into regular 4D components and extra-dimensional terms, and expressing it in terms of the longitudinal part of A_μ gives

$$\begin{aligned}
\mathcal{L}_e &= -\frac{1}{2}\mathrm{e}^{-\phi(z)}\Big[\sqrt{-g}g^{\mu\nu}(v^2\partial_\mu\pi\partial_\nu\pi + v^2\partial_\mu\varphi\partial_\nu\varphi - 2v^2\partial_\mu\pi\partial_\nu\varphi) \\
&\quad +\sqrt{-g}g^{zz}v^2\partial_z\pi\partial_z\pi + \frac{\sqrt{-g}g^{zz}g^{\mu\nu}}{g_5^2}(\partial_z\partial_\mu\varphi\partial_z\partial_\nu\varphi)\Big].
\end{aligned} \tag{2.16}$$

Varying (2.16) with respect to π and performing a Kaluza-Klein decomposition, as above in (2.6), expressing the system of equations in terms of its z-dependent parts.

$$e^\phi\partial_z\left(\frac{e^{-\phi}v^2}{z^3}\partial_z\pi_n\right) + \frac{v^2 m_n^2}{z^3}(\pi_n - \varphi_n) = 0. \tag{2.17}$$

Varying (2.16) with respect to φ and breaking it down into KK modes gives the second equation of motion

$$e^\phi\partial_z\left(\frac{e^{-\phi}}{z}\partial_z\varphi_n\right) + \frac{g_5^2 L^2 v^2}{z^3}(\pi_n - \varphi_n) = 0. \tag{2.18}$$

As usual, we express (2.17) and (2.18) in a Schrodinger-like form,

$$\pi = \mathrm{e}^{f(z)}\tilde{\pi} \qquad f(z) = \phi(z) + \log\frac{z^3}{v(z)^2} \tag{2.19}$$

$$\varphi = \mathrm{e}^{g(z)}\tilde{\varphi} \qquad g(z) = \phi(z) + \log z. \tag{2.20}$$

After reverting back to the notation $\tilde{\pi} \to \pi$ and $\tilde{\varphi} \to \varphi$ the equations of motion become

$$-\pi_n'' + \left(\frac{\phi'^2}{4} - \frac{\phi''}{2} - \frac{\phi'v'}{v} + \frac{3\phi'}{2z} + \frac{15}{4z^2} - \frac{3v'}{vz} + \frac{v''}{v} - m_n^2\right)\pi_n = -m_n^2\frac{v^2 L^2}{z^2}\varphi_n \tag{2.21}$$

$$-\varphi_n'' + \left(\frac{\phi'^2}{4} - \frac{\phi''}{2} + \frac{\phi'}{2z} + \frac{3}{4z^2} + \frac{g_5^2 v^2 L^2}{z^2}\right)\varphi_n = g_5^2\pi_n \tag{2.22}$$

Linear Representation

When considering the linear representation of the pseudoscalar field (2.14), there are terms quadratic and quartic in π that were not present in the exponential representation.

After making the appropriate substitutions in the Lagrangian, it becomes

$$
\begin{aligned}
\mathcal{L}_l &= -\frac{1}{2}e^{-\phi}\sqrt{-g}\Big(g^{\mu\nu}\partial_\mu\pi\partial_\nu\pi + g^{zz}\partial_z\pi\partial_z\pi - 2vg^{\mu\nu}\partial_\mu\pi\partial_\nu\varphi + m_X^2\pi^2 - \frac{\kappa}{2}v^2\pi^2 \\
&+ g^{\mu\nu}v^2\partial_\mu\varphi\partial_\nu\varphi + \frac{g^{\mu\nu}g^{zz}}{g_5^2}\partial_z\partial_\mu\varphi\partial_z\partial_\nu\varphi\Big).
\end{aligned}
\tag{2.23}
$$

Following the same procedure as above, we derive two coupled equations. Varying with respect to φ produces

$$
e^{\phi}\partial_z\left(\frac{e^{-\phi}}{z}\partial_z\varphi_n\right) + \frac{g_5^2L^2v}{z^3}\left(\pi_n - v\varphi_n\right) = 0.
\tag{2.24}
$$

Varying with respect to π gives the second equation of the linear representation

$$
z^3e^{\phi}\partial_z\left(\frac{e^{-\phi}}{z^3}\partial_z\pi_n\right) - \left(\frac{m_X^2}{z^2} - \frac{\kappa L^2v^2}{2z^2}\right)\pi_n + m_n^2\pi_n = m_n^2v\varphi_n.
\tag{2.25}
$$

We can express (2.24) and (2.25) in a Schrodinger-like form as above with the substitutions

$$
\pi_n = e^f\tilde{\pi}_n \qquad f = \frac{\chi}{2} + \frac{3}{2}\log\frac{z}{L}
\tag{2.26}
$$

$$
\phi_n = e^g\tilde{\phi}_n \qquad g = \frac{\chi}{2} + \frac{1}{2}\log\frac{z}{L}.
\tag{2.27}
$$

Simplifying the equations and reverting back to the notation $\tilde{\pi}_n \to \pi_n$ and $\tilde{\phi}_n \to \phi_n$ for simplicity, we find

$$
-\phi_n'' + \left(\frac{\phi'^2}{4} - \frac{\phi''}{2} + \frac{3}{4z^2} + \frac{\phi'}{2z} + \frac{g_5^2L^2v^2}{z^2}\right)\varphi_n = \frac{g_5^2Lv}{z}\pi_n
\tag{2.28}
$$

$$
-\pi_n'' + \left(\frac{\phi'^2}{4} - \frac{\phi''}{2} + \frac{3}{4z^2} + \frac{3\phi'}{2z} - \frac{\kappa L^2v^2}{2z^2} - m_n^2\right)\pi_n = -m_n^2\frac{vL}{z}\varphi_n
\tag{2.29}
$$

2.2.2 Representation Equivalence

The pseudoscalar field representation should not affect the physical results obtained from the model. It is therefore desirable to show that the equations of motion derived from the two representations are equivalent.

We begin by expanding X_e to first order in the fields

$$
\begin{aligned}
X_e &= \left(\frac{v}{2} + S\right)\left(1 + 2i\pi_e + \ldots\right) \\
&= \frac{v}{2} + S + i\pi_e v.
\end{aligned}
\tag{2.30}
$$

Comparing (2.30) to (2.14), we surmise that $\pi_e v(z) \to \pi_l$ is the relationship between the two representations. Let us substitute $\pi_e \to \pi_l/v(z)$ into the equations of motion of the exponential representation and attempt to obtain the equations of motion of the linear representation. The substitution into (2.18) immediately yields

$$e^\phi \partial_z \left(\frac{e^{-\chi}}{z} \partial_z \varphi \right) + \frac{g_5^2 v}{z^3}(\pi_l - v\varphi) = 0, \tag{2.31}$$

which is equivalent to (2.24) as expected. Showing the equivalence of the other two equations requires a bit more work. First we substitute for π_e in (2.17) and then simplify the expression,

$$\frac{z^3 e^\phi}{v} \partial_z \left(\frac{e^{-\phi} v^2}{z^3} \left(\frac{\pi_l'}{v} - \frac{\pi_l v'}{v^2} \right) \right) + m_n^2(\pi_l - v\varphi) = 0 \tag{2.32}$$

which becomes

$$\pi_l'' - \left(\phi' + \frac{3}{z} \right) \pi_l' - \frac{\pi_l}{v} \left(v'' - \phi'v' - \frac{3}{z}v' \right) + m_n^2(\pi_l - v\varphi) = 0. \tag{2.33}$$

Recalling the equation of motion for $v(z)$ (2.11), which does not depend on the pseuod-scalar representation:

$$v'' - \left(\phi' + \frac{3}{z} \right) v' + \left(\frac{3}{z^2} + \frac{\kappa L^2 v^2}{2z^2} \right) v = 0. \tag{2.34}$$

Using (2.34) in (2.33), we find

$$\pi_l'' - \left(\frac{3}{z} + \phi' \right) \pi_l' + \left(\frac{3}{z^2} + \frac{\kappa L^2 v^2}{2z^2} \right) \pi_l + m_n^2 \left(\pi_l - v\varphi \right) = 0, \tag{2.35}$$

which is equivalent to the other equation of motion of the linear representation (2.25). The equations of motion are equivalent, confirming that physical results do not depend on the representation.

2.2.3   Gell-Mann–Oakes–Renner Relation

In this section we explore the Gell-Mann–Oakes–Renner relation numerically. Inserting the established equivalence between the exponential and linear representations, $\pi_e = \pi_l/v(z)$, into (2.33), we obtain

$$\frac{g_5^2 L^2 v^2}{z^2} \partial_z \left(\frac{\pi_l}{v} \right) = m_\pi^2 \partial_z \varphi \,. \tag{2.36}$$

Following the method of [?], we construct a perturbative solution in m_π where $\varphi(z) = A(0, z) - 1$ and use the established relation

$$f_\pi^2 = - L \frac{\partial_z A(0, z)}{g_5^2 z} \bigg|_{z \to 0.} \tag{2.37}$$

Integrating (2.36) yields

$$\frac{\pi(z)}{v(z)} = m_\pi^2 \int_0^z du \, \frac{u^3}{v^2(u)} \frac{\partial_z A(0, u)}{g_5^2 u} \, . \tag{2.38}$$

The function $u^3/v^2(u)$ has significant support only at small values of $u \sim \sqrt{m_q/\sigma}$, where we may use (2.37) to relate the derivative on $A(0, u)$ to the pion decay constant, so that

$$\frac{\pi_l}{v} = - \frac{m_\pi^2 f_\pi^2}{2 m_q \sigma} \, . \tag{2.39}$$

We find that letting $\pi_l = -v(z)$ solves the axial-vector field's equation of motion

$$e^\phi \partial_z \left(\frac{e^{-\phi}}{z} \partial_z A_\mu(q, z) \right) - \frac{q^2}{z} A_\mu(q, z) - \frac{g_5^2 L^2 v^2}{z^3} A_\mu(q, z) = 0 \tag{2.40}$$

in the region of small z and as $q \to 0$. As a result, (2.39) becomes the expected Gell-Mann–Oakes–Renner (GOR) relation,

$$2 m_q \sigma = m_\pi^2 f_\pi^2 \, . \tag{2.41}$$

We solve for the ground-state pseudoscalar mass, m_π, for differing values of m_q to ensure that the numerical routine respects the GOR relation and gives a reasonable value for f_π. The results are plotted in Figure 2.1. We see linear behavior in the plot, indicating that as $m_q \to 0$ we obtain a constant ratio of m_q/m_π^2. The slope of the line in Figure 2.1 suggests $f_\pi = 90$ MeV, a result consistent with the input parameters as described in [?].
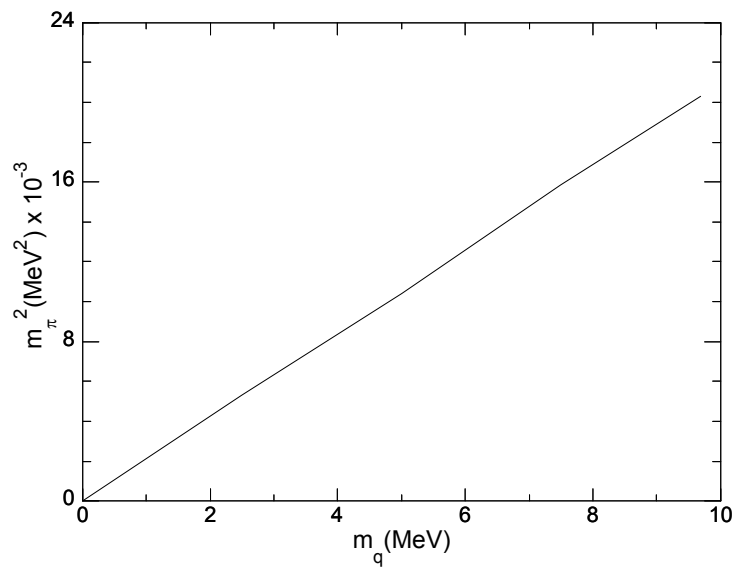
Figure 2.1: Plot of m_π^2 vs m_q yields a straight line from which the pion decay constant f_π is calculated using (2.41).

Chapter 3

Dynamical Three-Field Model

3.1 Review and Motivation

We assume that four-dimensional QCD can be modeled by the following five-dimensional action, written in the string frame:

$$S = \frac{1}{16\pi G_5} \int d^5x \sqrt{-g}\, e^{-2\Phi} \left(R + 4\partial_M \Phi \partial^M \Phi - \mathrm{Tr}\left[|DX|^2 + \partial_M \mathcal{G} \partial^M \mathcal{G} + \frac{1}{2g_5^2}(F_A^2 + F_V^2) + V_m(\Phi, X^2, \mathcal{G}) \right] \right)$$

(3.1)

where Φ is the dilaton and the metric is pure AdS, $g_{MN} = z^{-2}\eta_{MN}$, with the AdS curvature defined to be unity. The constant $g_5^2 = 12\pi^2/N_c$, where N_c is the number of colors. The covariant derivative is defined as $D_M = \partial_M + i[V_M, X] - i\{A_M, X\}$. The scalar field, X, which is dual to the $\bar{q}q$ operator, obtains a z-dependent vacuum expectation value (VEV):

$$\langle X \rangle = \frac{\chi(z)}{2} I,$$

(3.2)

where I is the 2×2 identity matrix. The glueball field $\mathcal{G}$ similarly obtains a z-dependent VEV, $G(z)$. We examine the background dynamics of the fields

$$S = \frac{1}{16\pi G_5} \int d^5x \sqrt{-g}\, e^{-2\Phi} \left(R + 4\partial_M \Phi \partial^M \Phi - \tfrac{1}{2}\partial_M \chi \partial^M \chi - \tfrac{1}{2}\partial_M G \partial^M G - V(\Phi, \chi, G) \right),$$

(3.3)

where $V = \mathrm{Tr}[V_m]$. The scalar fields Φ, χ, G are dimensionless.

It is easier to search for the background fields in the Einstein frame, where the

vacuum action takes the canonical form

$$\mathcal{S}_E = \frac{1}{16\pi G_5} \int d^5x \sqrt{-\tilde{g}} \left(\tilde{R} - \tfrac{1}{2}\partial_M\phi\partial^M\phi - \tfrac{1}{2}\partial_M\chi\partial^M\chi - \tfrac{1}{2}\partial_M G\partial^M G - \tilde{V}(\phi,\chi) \right).$$
(3.4)

The tilde distinguishes the two frames, with $\tilde{V} = e^{4\Phi/3}V$, and the dilaton is rescaled for a canonical action $\phi = \sqrt{8/3}\Phi$. The string and Einstein frame metrics are related by the conformal transformation

$$g_{MN} = e^{2\phi/\sqrt{6}}\tilde{g}_{MN}.$$
(3.5)

Previous work showed how to construct a potential for a gravity-dilaton-chiral system without the glueball condensate. We examine the behavior assuming that the fields have power-law behavior, which is accurate in both the UV and IR limits, [?]. One of the equations of motion is independent of the choice of potential,

$$\dot{\chi}^2 = \frac{\sqrt{6}}{z^2}\frac{d}{dz}(z^2\dot{\phi}).$$
(3.6)

To obtain linear confinement, the dilaton should have quadratic behavior in the IR limit, $\phi(z) = \lambda z^2$. The chiral field should have have linear behavior, $\chi(z) = Az$, where A sets the large-n mass splitting between the axial-vector and vector mesons in the model. This constant mass-splitting at large n occurs because of the non-restoration of chiral symmetry [?]. Inserting this into (3.6), we find that the chiral field behaves as

$$\chi(z) = 6^{3/4}\sqrt{\lambda}z,$$
(3.7)

which removes one of the independent parameters of the model in [?]. Using the phenomenological value of λ, which determines the slope of the Regge trajectories, we find a mass splitting that is much too large.

Because this problem arises in the equation that is independent of the potential, this issue cannot be resolved by the choice of potential in models that do not consider the glueball condensate. Models that derive the field behavior using the superpotential method suffer from the same problem.

To resolve this problem, we consider the effects of the glueball condensate G on the background equations. This field must be linear in the IR for linear confinement, and go as $G \sim z^4$ in the UV to match the operator dimension in the AdS/CFT dictionary.

It is noted that the model proposed by Huang and Li [**?**, **?**] accurately models the non-restoration of chiral symmetry using a model with only two background fields, but their model differs from the work presented here in several respects. They place the meson fields and chiral dynamics in the open-string sector of the model. For linear confinement, this requires that the chiral field approach a constant in the IR, which necessitates a modified metric to obtain the correct chiral dynamics. Our model allows the metric to remain purely AdS in the string frame. Finally, they do not determine an explicit form of the potential, which is the central goal of this work.

3.2   Construction of Potential

Consider the action in the Einstein frame (3.4). To simplify the equations of motion, we use a transformed potential,

$$V = e^{-2\phi/\sqrt{6}}\tilde{V}. \tag{3.8}$$

It is noted that this is simply the potential in the string frame. We re-write the potential as

$$V = -12 + 4\sqrt{6}\phi + a_0\phi^2 + \frac{m_X^2}{2}\chi^2 + U. \tag{3.9}$$

Here U is more than quadratic in the fields. The AdS/CFT dictionary sets the mass for the fields according to the dimension of the dual operator,

$$m^2L^2 = \Delta(\Delta - 4). \tag{3.10}$$

The dimension of the $q\bar{q}$ operator is 3, so $m_X^2 = -3/L^2$. The dilaton mass is undetermined and is not connected to the dimension of the corresponding operator, as discussed in [**?**]. It is related to the parameter a_0 by $a_0 = \frac{1}{2}\left[(m_\phi L)^2 - 8\right]$. The potential should be an even function of χ.

The equations of motion can be written as

$$\dot{\chi}^2 + \dot{G}^2 = \frac{\sqrt{6}}{z^2}\frac{d}{dz}(z^2\dot{\phi}) \tag{3.11}$$

$$U = \frac{1}{2}\sqrt{6}z^2\ddot{\phi} - \frac{3}{2}(z\dot{\phi})^2 - 3\sqrt{6}z\dot{\phi} - 4\sqrt{6}\phi - a_0\phi^2 + \frac{3}{2}\chi^2 \tag{3.12}$$

$$\frac{\partial U}{\partial \phi} = 3z\dot{\phi} - 2a_0\phi \tag{3.13}$$

$$\frac{\partial U}{\partial \chi} = z^2 \ddot{\chi} - 3z\dot{\chi}\left(1 + \frac{z\dot{\phi}}{\sqrt{6}}\right) + 3\chi \tag{3.14}$$

$$\frac{\partial U}{\partial G} = z^2 \ddot{G} - 3z\dot{G}\left(1 + \frac{z\dot{\phi}}{\sqrt{6}}\right) \tag{3.15}$$

We assume that the potential has no explicit dependence on the coordinate z, so the equations 3.13-3.15 are not independent, and we can eliminate one.

3.2.1   IR Limit

The requirement of linear confinement requires a solution in the large z limit of the form

$$\phi = \lambda z^2 \tag{3.16}$$

$$\chi = Az \tag{3.17}$$

$$G = Bz. \tag{3.18}$$

Substitution into (3.11) gives
$$A^2 + B^2 = 6\sqrt{6}\lambda \tag{3.19}$$

The λ is fixed by the slope of the linear trajectory and A is fixed by the axial-vector – vector mass difference. It is useful to write these as

$$A = 6^{3/4}\sqrt{\lambda}\cos\theta$$

$$B = 6^{3/4}\sqrt{\lambda}\sin\theta, \tag{3.20}$$

where θ now becomes the parameter controlling the axial-vector – vector mass splitting. Inserting (3.18) into (3.12-3.15) suggests the following terms in our ansatz for the potential

$$U = a_1\phi\chi^2 + a_2\phi G^2 + a_3\chi^4 + a_4 G^4 + a_5\chi^2 G^2 + a_6 G^2 \tanh(g\phi). \tag{3.21}$$

We see that there must be a G^2 term in the IR limit, but this is forbidden in the weak-field limit because the glueball condensate field is massless. To circumvent this, we propose the term $G^2 \tanh(g\phi)$ with $g > 0$. In the weak field limit this goes to $g\phi G^2$, which is acceptable. The tanh is suggested by 3.8, and it suggests a rapid

exponential transition from the weak field to the strong field limits that is supported by phenomenology. By substitution one finds the following constraints on the parameters:

$$U \to 6 + a_0 + 6\sqrt{6}\left(\cos^2\theta\, a_1 + \sin^2\theta\, a_2\right)$$

$$+6^3\left(\cos^4\theta\, a_3 + \sin^4\theta\, a_4 + \cos^2\theta \sin^2\theta\, a_5\right) = 0 \tag{3.22}$$

$$\frac{\partial U}{\partial \chi} \to 2a_1 + 24\sqrt{6}\cos^2\theta\, a_3 + 12\sqrt{6}\sin^2\theta\, a_5 + \sqrt{6} = 0 \tag{3.23}$$

$$\frac{\partial U}{\partial G} \to 2a_2 + 24\sqrt{6}\sin^2\theta\, a_4 + 12\sqrt{6}\cos^2\theta\, a_5 + \sqrt{6} = 0 \tag{3.24}$$

$$\frac{\partial U}{\partial G} \to a_6 = -\frac{3}{2} \tag{3.25}$$

We have chosen to exclude (3.13) because it is not independent. The parameter a_6 is determined, and the others will be determined by an examination of the UV limit.

3.2.2   UV Limit

Next we look for a solution in the small z limit. The AdS/CFT dictionary dictates that the leading-order UV behavior of the chiral and glueball condensate fields is determined by their dimension. Note also that we are working in the chiral limit where the quark mass is zero. We start by examining only the leading-order terms

$$\chi = \Sigma_0 z^3 \tag{3.26}$$

$$G = G_0 z^4. \tag{3.27}$$

Substitution into (3.11) and imposing the boundary condition $\phi(0) = 0$ gives

$$\phi = \frac{\sqrt{6}}{28}\Sigma_0^2 z^6 + \frac{\sqrt{6}}{27}G_0^2 z^8 \tag{3.28}$$

Using only this leading-order behavior in (3.12-3.15), the system of equations is inconsistent, as there are more equations from matching powers of z than unknown parameters.

To solve this problem, try adding a term $\Sigma_n z^n$ to χ. Substituting into (3.11) and keeping only the lowest-order cross-term we find the additional term in ϕ

$$\Delta\phi = \frac{\sqrt{6}\, n\Sigma_0\Sigma_n}{(n+4)(n+3)}z^{n+3} \tag{3.29}$$

From (3.12) we find that

$$U = -\tfrac{3}{2}(z\dot{\phi})^2 - a_0\phi^2 + 3\frac{n^3 - 13n + 12}{(n+4)(n+3)}\Sigma_0\Sigma_n z^{n+3} \qquad (3.30)$$

Since the ϕ^2 terms start out as z^{12}, z^{14}, z^{16}, and so do the terms in the potential, the n can only take the values 9, 11, etc. This term contributes only to the equation for $\partial U/\partial\chi$.

$$\frac{\partial U}{\partial \chi} = -9\Sigma_0 \left(\frac{3}{14}\Sigma_0^2 + \frac{8}{27}G_0^2 z^2\right) z^9 + (n-3)(n-1)\Sigma_n z^n \qquad (3.31)$$

By power counting both $n = 9$ and $n = 11$ can contribute.

There could also be higher order terms in G such as $G_m z^m$. This leads to the additional term in ϕ

$$\Delta\phi = \frac{8mG_0 G_m}{\sqrt{6}(m+5)(m+4)} z^{m+4} \qquad (3.32)$$

It contributes to the equation for $\partial U/\partial G$ as

$$\frac{\partial U}{\partial G} = -12G_0 \left(\frac{3}{14}\Sigma_0^2 + \frac{8}{27}G_0^2 z^2\right) z^{10} + m(m-4)G_n z^m \qquad (3.33)$$

The choice $m = 8$ is not possible as there is no term of the same order to balance it. Terms with $m = 10$ and $m = 12$ are possible. These new terms cannot affect the equation for $\partial U/\partial\phi$ nor can they contribute to the equation for $\partial U/\partial\chi$. Considering higher order terms in both χ and G leads to

$$U = -\tfrac{3}{2}(z\dot{\phi})^2 - a_0\phi^2 + 3\frac{n^3 - 13n + 12}{(n+4)(n+3)}\Sigma_0\Sigma_n z^{n+3} + \frac{4m(m-4)}{m+4}G_0 G_m z^{m+4} \qquad (3.34)$$

The appearance of these terms can be understood by writing the following schematic expansions.

$$\chi \sim \Sigma_0 z^3 + \Sigma_0^3 z^9 + G_0^2\Sigma_0 z^{11} + \cdots$$

$$G \sim G_0 z^4 + \Sigma_0^2 G_0 z^{10} + G_0^3 z^{12} + \cdots$$

That is, χ is an odd function of Σ_0 and G is an odd function of G_0. These are the symmetries in the equations of motion. They also follow the spirit of the AdS/CFT correspondence in terms of the dimensionality of the operators and the powers of z.

Including now $m = 10$ and 12, and $n = 9$ and 11, we have the following set of equations in the small z limit:

$$
\begin{aligned}
U_{\text{LHS}} &= 3\Sigma_0^4 z^{12}\left[4\frac{\Sigma_9}{\Sigma_0^3} - \frac{(54 + a_0)}{2^3 \cdot 7^2}\right] \\
&+ \frac{1}{7}\Sigma_0^2 G_0^2 z^{14}\left[120\frac{G_{10}}{\Sigma_0^2 G_0} + 120\frac{\Sigma_{11}}{\Sigma_0 G_0^2} - \frac{(72 + a_0)}{9}\right] \\
&+ 2G_0^4 z^{16}\left[12\frac{G_{12}}{G_0^3} - \frac{(96 + a_0)}{3^5}\right]
\end{aligned}
\tag{3.35}
$$

$$
\begin{aligned}
U_{\text{RHS}} &= \Sigma_0^4 z^{12}\left[\frac{\sqrt{6}}{28}a_1 + a_3\right] \\
&+ \Sigma_0^2 G_0^2 z^{14}\left[\frac{\sqrt{6}}{27}a_1 + \frac{\sqrt{6}}{28}(a_2 + ga_6) + a_5\right] \\
&+ G_0^4 z^{16}\left[\frac{\sqrt{6}}{27}(a_2 + ga_6) + a_4\right]
\end{aligned}
\tag{3.36}
$$

$$
\left(\frac{\partial U}{\partial \chi}\right)_{\text{LHS}} = 3\Sigma_0^3 z^9\left[-\frac{9}{14} + 16\frac{\Sigma_9}{\Sigma_0^3}\right] + 8\Sigma_0 G_0^2 z^{11}\left[-\frac{1}{3} + 10\frac{\Sigma_{11}}{\Sigma_0 G_0^2}\right]
\tag{3.37}
$$

$$
\left(\frac{\partial U}{\partial \chi}\right)_{\text{RHS}} = \Sigma_0^3 z^9\left[\frac{\sqrt{6}}{14}a_1 + 4a_3\right] + \Sigma_0 G_0^2 z^{11}\left[\frac{2\sqrt{6}}{27}a_1 + 2a_5\right]
\tag{3.38}
$$

$$
\left(\frac{\partial U}{\partial G}\right)_{\text{LHS}} = 6\Sigma_0^2 G_0 z^{10}\left[-\frac{3}{7} + 10\frac{G_{10}}{\Sigma_0^2 G_0}\right] + 32G_0^3 z^{12}\left[-\frac{1}{9} + 3\frac{G_{12}}{G_0^3}\right]
\tag{3.39}
$$

$$
\left(\frac{\partial U}{\partial G}\right)_{\text{RHS}} = \Sigma_0^2 G_0 z^{10}\left[\frac{\sqrt{6}}{14}(a_2 + ga_6) + 2a_5\right]
\tag{3.40}
$$

$$
+ G_0^3 z^{12}\left[\frac{2\sqrt{6}}{27}(a_2 + ga_6) + 4a_4\right]
\tag{3.41}
$$

Altogether, from both the UV and IR limits, there are ten independent equations for the twelve parameters $a_0 - a_6$, Σ_9, Σ_{11}, G_{10}, G_{12}, and g. We take g as the free parameter to use as the rate of transition from small z to large z. The parameters in the potential are found to be

$$
a_0 = \frac{3}{2}\frac{1}{6 + \sin^2\theta}\left[120 + 62\sin^2\theta + 63\sqrt{6}g\sin^2\theta\right]
\tag{3.42}
$$

$$a_1 = -\frac{3\sqrt{6}}{4}\frac{1}{6+\sin^2\theta}\left[12 + 8\sin^2\theta + 9\sqrt{6}g\sin^2\theta\right] \tag{3.43}$$

$$a_2 = -\frac{\sqrt{6}}{4}\frac{1}{6+\sin^2\theta}\left[32 + 24\sin^2\theta + 3\sqrt{6}g(9\sin^2\theta - 2)\right] \tag{3.44}$$

$$2a_3\cos^2\theta + a_5\sin^2\theta = \frac{1}{24}\frac{1}{6+\sin^2\theta}\left[24 + 22\sin^2\theta + 27\sqrt{6}g\sin^2\theta\right] \tag{3.45}$$

$$2a_4\sin^2\theta + a_5\cos^2\theta = \frac{1}{24}\frac{1}{6+\sin^2\theta}\left[20 + 22\sin^2\theta + 3\sqrt{6}g(9\sin^2\theta - 2)\right] \tag{3.46}$$

$$a_6 = -\frac{3}{2} \tag{3.47}$$

The coefficients a_0, a_1, a_2 and a_6 are determined, while there are two equations for the three coefficients a_3, a_4 and a_5. That leaves a_5 as a free parameter, to be fit numerically, along with g, θ, G_0, Σ, and λ.

3.3   Numerical Solution

Using the above potential, we seek a numerical solution that simultaneously satisfies the UV and IR limits. We use equations (3.11, 3.14, 3.15), which allows for an additional term in the potential, ΔU, such that

$$\frac{\partial}{\partial\chi}\Delta U = \frac{\partial}{\partial G}\Delta U = 0, \tag{3.48}$$

which will be determined from the numerical solution.

The differential equations represent a stiff system, and treatment of the problem as an initial value problem leads to numerical instabilities. We treat it instead as a boundary value problem, using Dirichlet boundary conditions at both boundaries. A relaxation method is used in combination with input approximations for the background fields, which are then iterated to find a stable solution to the system with the given boundary conditions. Because the system is nonlinear, the solution found is not guaranteed to be unique.

The IR boundary is chosen to be sufficiently large to capture the infrared behavior and to give accurate Regge behavior large-n radial excitations of the mesons. The UV boundary should approach zero, but it cannot reach zero because of the singularity

in the equations of motion. This becomes a problem because equation (3.11) allows constant and divergent terms

$$\Delta\phi(z) = c_1 + c_2 z^{-1}. \tag{3.49}$$

Symbolically, these terms can be set to zero by enforcing the Dirichlet boundary condition $\phi(0) = 0$, but this is impossible to enforce numerically. Creative choice of UV boundary conditions can eliminate one, but not both of these unwanted terms without affecting the chiral and glueball fields. The behavior of the numerical solutions suggests that the desired UV behavior is an unstable solution to the equations, and therefore difficult or impossible to find with this iterative method.

As an alternative to direct solution, we parameterize the fields as follows:

$$\Psi(z) = \psi(z)_{UV} f(z) + \psi(z)_{IR} \left(1 - f(z)\right), \tag{3.50}$$

where $f(z)$ is some function that transitions smoothly from 1 at small values of z to 0 at large z, and $\psi(z)_{xx}$ represents the known UV and IR limits of the fields ϕ, χ, and G. The switching functions f need not be the same for each field. We choose

$$f_\phi(z) = e^{-(\beta_1 z)^{10}} \tag{3.51}$$
$$f_\chi(z) = e^{-(\beta_2 z)^4} \tag{3.52}$$
$$f_G(z) = e^{-(\beta_3 z)^5}. \tag{3.53}$$

The powers of the exponential are chosen to be greater than the known power-law behavior of the fields in the UV limit, so as to not interfere with this behavior. The β_i will be set by numerical fitting.

The chiral condensate Σ is set using the Gell-Mann–Oakes–Renner relation:

$$(m_u + m_d)\Sigma = f_\pi^2 m_\pi^2. \tag{3.54}$$

Using $m_\pi = 139.6$ MeV, $f_\pi = 92$ MeV, and $m_u + m_d = 7.0$ MeV yields a value of $\Sigma = (286\,\text{MeV})^3$.

In all, we have eight parameters to be set numerically. The first constraint is to obtain the best global visual fit to the meson spectrum. We do not simply do a chi-squared fitting to the experimental data because the measurement error for the ground

state ρ meson is so much smaller than for the others that this would effectively act as the only constraint. Secondly, we seek to minimize the error in the finite-difference approximations to equations $3.11, 3.14$, and 3.15.

Three of the parameters are most phenomenologically relevant: λ, which controls the slope of the meson spectra in the large-n limit; θ, which controls the mass splitting between the a_1 and ρ mesons, and β_2, which controls the location of the "bend" in the a_1 spectrum. For each set of these parameters, the other parameters are set by a routine that minimizes the error in the equations of motion. The parameters found are shown in Table 3.1.
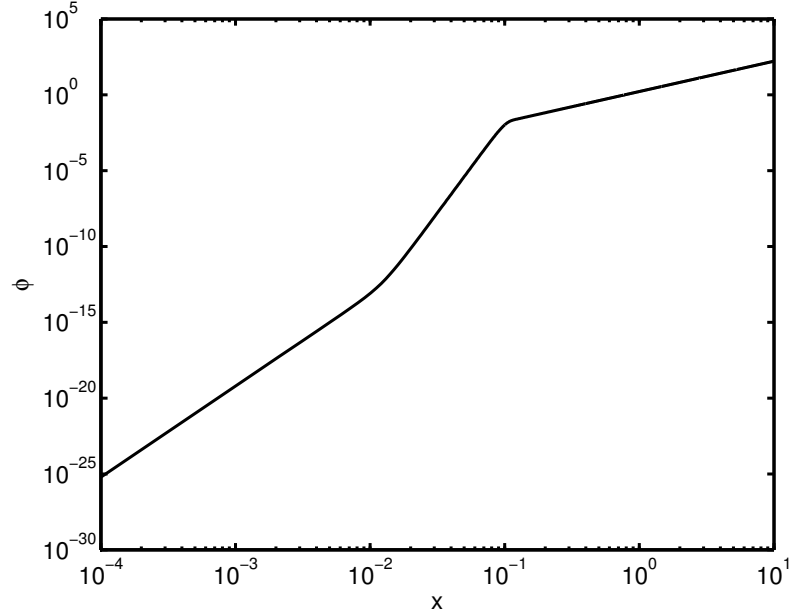

Figure 3.1: A plot of the dilaton field Φ generated by the parameterization (3.52). The UV and IR asymptotic behavior is apparent. The coordinate x is a dimensionless re-scaling of the conformal coordinate, $x = \sqrt{\lambda}z$.

The background fields that are obtained from this analysis are shown in Figures 3.1-3.3. The asymptotic power-law behavior of the fields is evident in the linear portions of the log-log scale plots shown. The "transition" behavior is most evident in the dilaton because of the large value of β_1, which controls the value of z at which the field transitions from the UV limit to the IR limit.
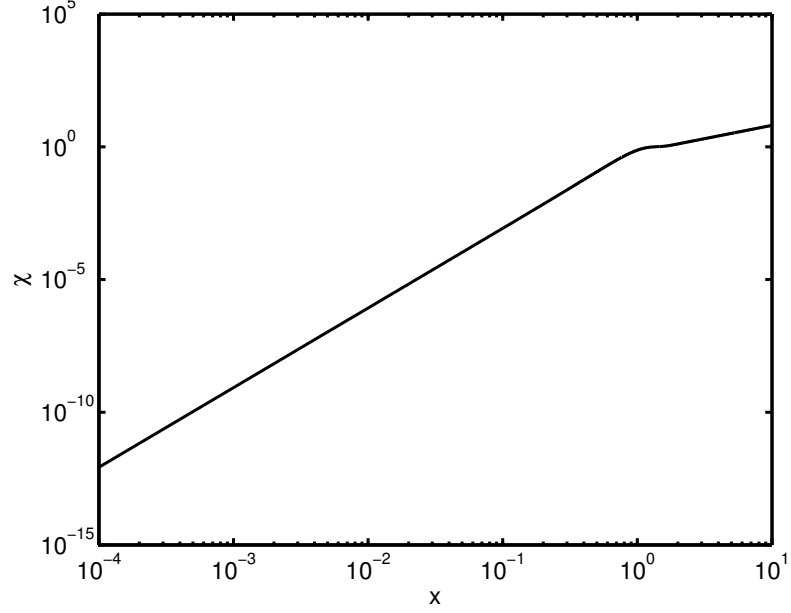
Figure 3.2: A plot of the chiral field χ generated by the parameterization (3.53). The UV and IR asymptotic behavior is apparent, with a rapid transition between them. The coordinate x is a dimensionless re-scaling of the conformal coordinate, $x = \sqrt{\lambda}z$.

We now analyze the "extra" term in the potential, ΔU. We obtain this term numerically by subtracting the right-hand side of 3.12 from its left-hand side. This term can be approximated numerically as a function of the dilaton field,

$$\Delta U(\Phi) = \alpha_1 \Phi^2 e^{-(\Phi-\gamma 1)^2/\delta 1} + \alpha_2 \Phi^2 e^{-(\Phi-\gamma_2)^2/\delta_2}. \qquad (3.55)$$

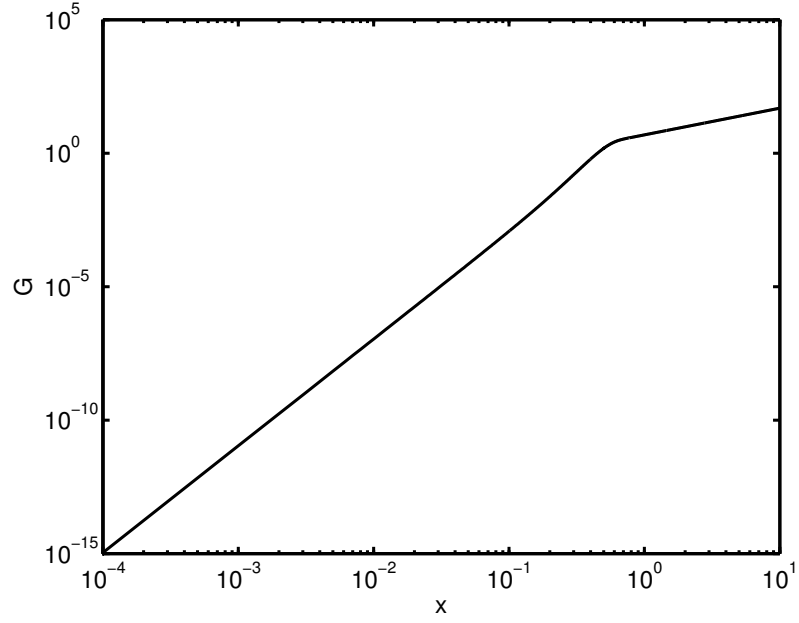The best-fit values for these parameters are shown in Table 3.3.

Figure 3.3: A plot of the glueball field G generated by the parameterization (3.53). The UV and IR asymptotic behavior is apparent, with a rapid transition between them. The coordinate x is a dimensionless re-scaling of the conformal coordinate, $x = \sqrt{\lambda}z$.

$\lambda^{1/2}$	304 MeV	β_1	3.04 GeV
$G_0^{1/4}$	552 MeV	β_2	274 MeV
θ	1.44	β_3	558 MeV
g	3.20	a_5	1.63

Table 3.1: Best fit parameters for the phenomenological model. The parameters λ, θ, and β_2 are chosen for the best visual fit to the ρ and a_1 data, with the rest set by minimizing the error in the equations of motion (3.11), (3.14-3.15).
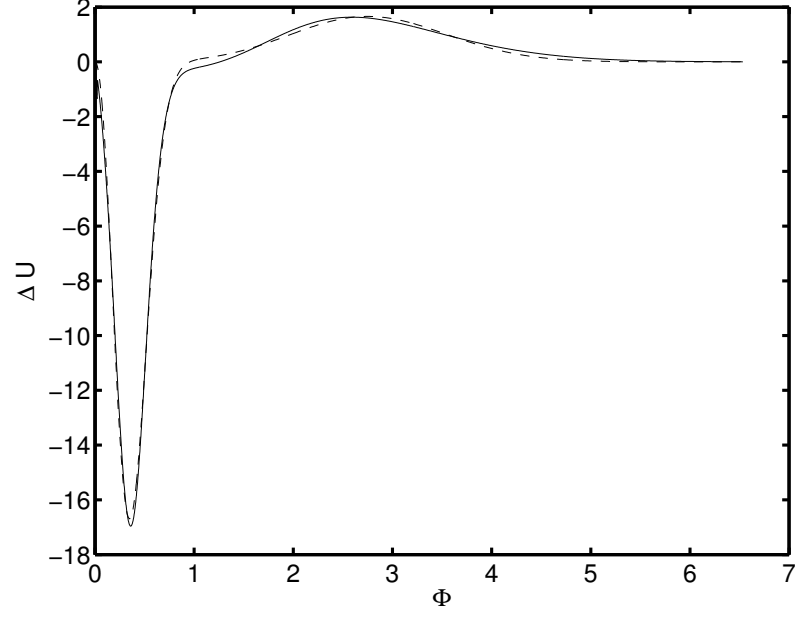
Figure 3.4: Plot of the "extra" term in the potential, $\Delta U(\phi)$. The solid line represents the numerical result, while the dashed line is the fitting of (3.55) using the parameters of Table 3.3.

α_1	-304.3 $\pm$ 5 $\times 10^{-1}$
γ_1	0.07086 $\pm$ 4 $\times 10^{-3}$
δ_1	0.09699 $\pm$ 1.3 $\times 10^{-3}$
α_2	0.2671 $\pm$ 6.4 $\times 10^{-3}$
γ_2	2.213 $\pm$ 4 $\times 10^{-2}$
δ_2	1.471 $\pm$ 9 $\times 10^{-2}$

Table 3.2: The dimensionless parameters for the fitting to ΔU

Chapter 4

Meson Spectra

To calculate the spectra of the radial excitations of the mesons, we examine the relevant terms from the string frame action (3.1),

$$\mathcal{S}_{meson} = -\frac{1}{16\pi G_5} \int d^5x \sqrt{-g} e^{-2\Phi} \text{Tr} \left[|DX|^2 + V_m(\Phi, X^2, \mathcal{G}) + \frac{1}{2g_5^2} \left(F_A^2 + F_V^2 \right) \right].$$
(4.1)

The 2×2 scalar field X contains the scalar and pseudoscalar fields (S, π), as well as the VEV.

We find the equations of motion for the various meson fields by varying the meson action. For the vector and axial-vector fields, we assume that the Kaluza-Klein modes are separable from the 4D parts of the fields. The equation of motion in the axial gauge $\Psi_5 = 0$ is given by

$$-\partial_z^2 \Psi_n + \omega' \partial_z \Psi_n + M_\Psi^2(z) \Psi_n = m_{\Psi_n}^2 \Psi_n,$$
(4.2)

where $\omega = 2\Phi(z) + log(z)$. The z-dependent mass term coefficient $M_V^2 = 0$ for the vector field, and

$$M_A^2 = \frac{g_5^2 L^2 \chi^2}{z^2}$$
(4.3)

for the axial field. The equation can be put in the Schrödinger form with the substitution $\Psi_n = e^{\omega/2}\psi_n$, resulting in

$$-\partial_z^2 \psi_n + \left(\tfrac{1}{4}\omega'^2 - \tfrac{1}{2}\omega'' + M_\psi^2 \right) \psi_n = m_{\Psi_n}^2 \psi_n.$$
(4.4)

These equations are analytically solvable in the IR limit, but full analysis requires the use of a numerical shooting method to find the mass eigenvalues. This model finds a better phenomenological fit than the results presented in [**?**], particularly for the ground state ρ meson, as shown in Figure 4.2. The scalar mesons are expected to mix with the scalar glueball field of this model, and this analysis is not performed here.
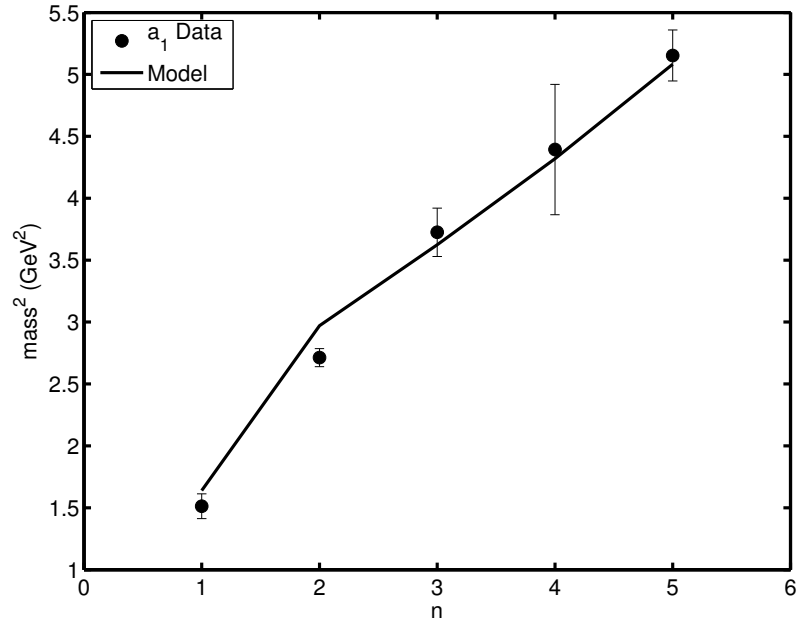

Figure 4.1: Comparison of the predicted mass eigenvalues for the axial-vector sector with the experimental a_1 meson spectrum [**?**].

n	a_1 experimental (MeV)	a_1 model
1	1230 ± 40	1280
2	1647 ± 22	1723
3	$1930 \, ^{+30}_{-70}$	1904
4	2096 ± 122	2078
5	$2270 \, ^{+55}_{-40}$	2254

Table 4.1: The experimental and predicted values for the masses of the axial-vector mesons.
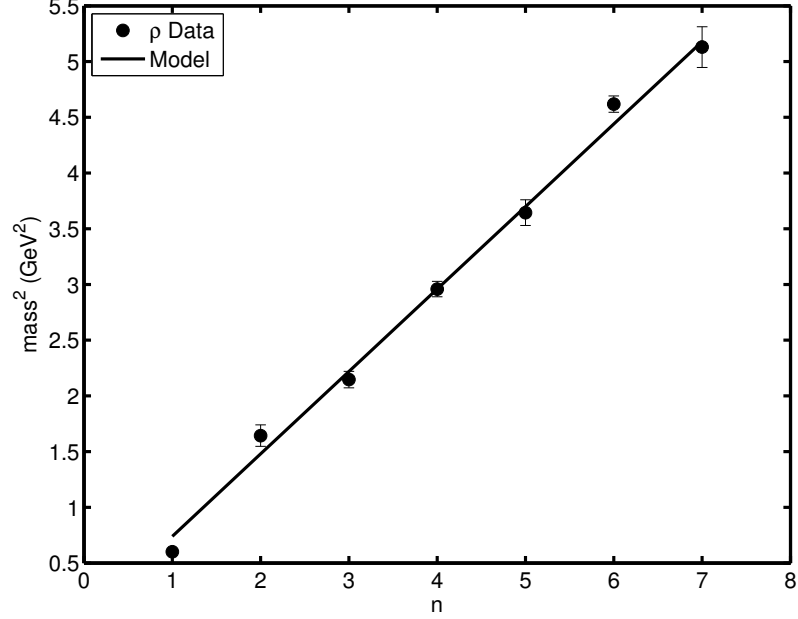
Figure 4.2: Comparison of the predicted mass eigenvalues for the vector sector with the experimental ρ meson spectrum [?].

4.1 Pseudoscalar Sector

When using the exponential representation for the scalar field, the terms from the potential do not contribute to the equations of motion for the pion field. This can be easily seen by noting that $|X_e|^n$ does not contain any terms involving the π_e field when n is even. We have required the potential to be an even function of X, so there are no such terms. This would seem to suggest that we use the exponential representation to calculate the pion mass spectrum. However, as noted in [?], π_e is extremely sensitive to boundary conditions, and the numerical results are not reliable. For this reason, we seek to work with an equation of motion written in the linear representation.

For convenience, we begin by deriving the equations of motion in the exponential representation. Working in the axial gauge $A_z = 0$, we rewrite the axial meson field in terms of its perpendicular and longitudinal components: $A_\mu = A_{\mu\perp} + \partial_\mu\varphi$. Only the longitudinal component of the axial field, φ, contributes to the pion equations of

n	ρ experimental (MeV)	ρ model
1	775.5 ± 1	860
2	1282 ± 37	1216
3	1465 ± 25	1489
4	1720 ± 20	1720
5	1909 ± 30	1923
6	2149 ± 17	2107
7	2265 ± 40	2276

Table 4.2: The experimental and predicted values for the masses of the vector mesons.

motion. We use (4.1), keeping only the relevant terms

$$\mathcal{L} = e^{-2\Phi}\sqrt{-g}[\chi^2(\partial_\mu \pi_e \partial^\mu \pi_e + \partial_\mu \varphi \partial^\mu \varphi - 2\partial_\mu \pi \partial^\mu \varphi + \partial_z \pi_e \partial^z \pi_e) \tag{4.5}$$
$$+ \frac{1}{g_5^2}\partial_z \partial_\mu \varphi \partial^z \partial^\mu \varphi].$$

Varying with respect to φ yields

$$e^{2\Phi}\partial_z\left(\frac{e^{-2\Phi}}{z}\partial_z\varphi\right) + \frac{g_5^2\chi^2}{z^3}(\pi_e - \varphi) = 0, \tag{4.6}$$

while varying π_e gives

$$\frac{e^{2\Phi}z^3}{\chi^2}\partial_z\left(\frac{e^{-2\Phi}\chi^2}{z^3}\partial_z\pi_e\right) + m_n^2(\pi_e - \varphi) = 0. \tag{4.7}$$

It was shown in [?] that the equations of motion are equivalent under the substitution $\pi_e \to \pi_l/\chi(z)$, so we make the appropriate substitution and expand the equations:

$$-\varphi'' + \left(2\Phi' + \frac{1}{z}\right)\varphi' = \frac{g_5^2\chi}{z^2}(\chi\varphi - \pi_l) \tag{4.8}$$

$$-\pi_l'' + \left(2\Phi' + \frac{3}{z}\right)\pi_l' + \left(\chi'' - 2\chi'\Phi' - \frac{3\chi'}{z}\right)\frac{\pi_l}{\chi} = m_n^2(\pi_l - \chi\varphi). \tag{4.9}$$

We can put these equations into Schödinger-like form with the following substitutions

$$\varphi = e^{\omega/2}\varphi_n \tag{4.10}$$
$$\pi_l = e^{\omega_s/2}\pi_n, \tag{4.11}$$

with $\omega = 2\Phi + \log(z)$ and $\omega_s = 2\Phi + 3\log(z)$. This yields

$$-\varphi_n'' + \left(\tfrac{1}{4}\omega'^2 - \tfrac{1}{2}\omega'' + \frac{g_5^2\chi^2}{z^2}\right)\varphi_n = \frac{g_5^2\chi}{z}\pi_n \tag{4.12}$$

$$-\pi_n'' + \left(\tfrac{1}{4}\omega_s'^2 - \tfrac{1}{2}\omega_s'' + \frac{\chi''}{\chi} - \frac{2\chi'\Phi'}{\chi} - \frac{3\chi'}{z\chi} - m_n^2 \right) \pi_n = -m_n^2 \frac{\chi}{z}\varphi_n. \tag{4.13}$$

The dependence of these equations of motion on the scalar potential can be made explicit by using the background equation for the chiral field, written here in the string frame

$$z^2\chi'' - 3z\chi' \left(1 + \frac{z\Phi'}{\sqrt{6}} \right) = m_X^2\chi + \frac{\partial U}{\partial \chi}. \tag{4.14}$$

Substituting, we can re-write (4.13) as

$$-\pi_n'' + \left(\tfrac{1}{4}\omega_s'^2 - \tfrac{1}{2}\omega_s'' + \frac{m_X^2}{z^2} + \frac{1}{z^2}\frac{\partial U}{\partial \chi} - m_n^2 \right) \pi_n = -m_n^2 \frac{\chi}{z}\varphi_n \tag{4.15}$$
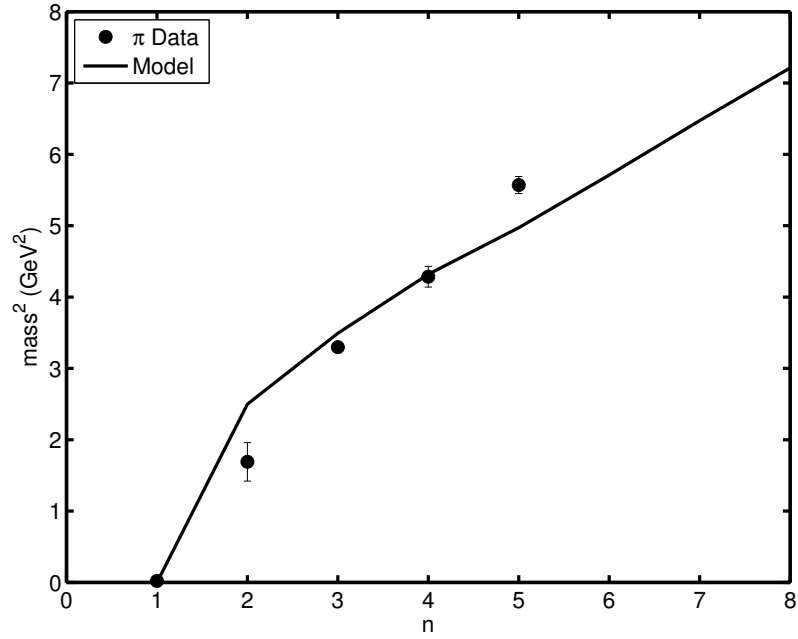

Figure 4.3: Comparison of the predicted mass eigenvalues for the scalar sector with the experimental π meson spectrum.

n	π experimental (MeV)	π model
1	140	0
2	1300 ± 100	1580
3	1816 ± 14	1868
4	$2070 \pm 35^*$	2078
5	$2360 \pm 25^*$	2230
6	–	2389
7	–	2544
8	–	2686

Table 4.3: The experimental and predicted values for the masses of the pseudoscalar mesons. *Appears only in the further states of the PDG.

Chapter 5

Conclusion and Discussion

Appendix A

Numerical Methods for solving Ordinary Differential Equations

Ordinary differential equations can always be reduced to a system of coupled first-order differential equations, which is advantageous for numerical solutions. For example, the second-order equation

$$y''(x) + f(x)y'(z) = g(x) \tag{A.1}$$

can be rewritten as

$$y'(x) = z(x) \tag{A.2}$$

$$z'(x) = g(z) - f(x)z(x) \tag{A.3}$$

Written generically, an ordinary differential equations system is reduced to a set of N first-order differential equations

$$y_i'(x) = f_i(x, y1, \ldots, y_N) \qquad i = 1, \ldots, N \tag{A.4}$$

where the functions f_i are some known set of equations involving the coordinate x and the dependent variables y_i. For a unique solution, one must specify a set of N boundary conditions. If these conditions are all specified at a single point, x_0, this is known as an initial value problem, and one can simply choose an integration method and calculate the values for f_i over the desired domain. When some of the conditions are specified at point x_0 and the rest are specified at the point x_f, this is known as a boundary value problem, and one must use one of the methods detailed below.

A.1 Shooting Method

The shooting method turns boundary value problems into initial value problems. The classic example of a shooting method can be visualized as the firing of a cannon, with boundary conditions given by the location of the cannon and the location of the target. This is changed to an initial value problem by selecting an arbitrary value for the angle of the cannon and firing. The angle of the cannon is incremented until the cannonball hits the target, which matches the final boundary condition.

More concretely, the boundary value problem is written as in (A.4), with boundary conditions

$$B_{1j}(x_0, y_1, \ldots, y_N) = 0 \qquad j = 1, \ldots, n_1 \tag{A.5}$$

$$B_{2k}(x_f, y_1, \ldots, y_N) = 0 \qquad k = 1, \ldots, n_2 \tag{A.6}$$

with n_1 boundary conditions at point x_0 and $n_2 = N - n_1$ at point x_f. These boundary conditions generically can be any algebraic combination of the variables.

For concreteness, consider a second-order eigenvalue problem of the type considered in this thesis,

$$\psi_n''(z) + V(z)\psi_n(z) = m_n^2 \psi_n(z). \tag{A.7}$$

This can be reduced to two first-order differential equations by making the substitutions $y_1 = \psi$, $y_2 = \psi'$, resulting in the system

$$y_1' = y_2 \tag{A.8}$$

$$y_2' = \left(m_n^2 - V(z)\right) y_1. \tag{A.9}$$

The boundary conditions are $y_1(z_0) = y_1(z_f) = 0$. [1]   In this instance, the eigenvalues are of greater importance than the behavior of the solutions y_1, y_2, so the overall normalization of the solutions is arbitrary.

This boundary value problem is changed to an initial value problem by setting

$$y_1(z_0) = 0 \tag{A.10}$$

$$y_2(z_0) = c, \tag{A.11}$$

---

[1] In the soft-wall model, we should take the limit $z_f \to \infty$. This is impossible to do numerically, but it is easy to make z_f sufficiently large that the eigenvalues are not effected.

where c is an arbitrary constant. A small test value for m_n is chosen, and the initial value problem is solved.
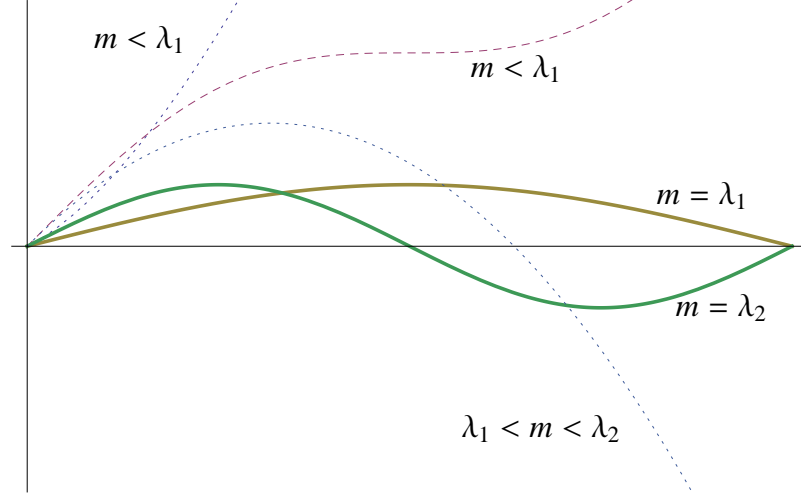

Figure A.1: An illustration of the shooting method.

As illustrated in Figure A.1, when the test value for m_n is less than the first eigenvalue λ_1, the value of $y_1(x_f)$ is positive. As m_n is incremented, eventually $y_1(x_f)$ becomes negative. A root-finding routine is used to approximate the values λ_n such that $y_1(x_f) = 0$. The number of antinodes in the wavefunction indicates to which excitation mode the eigenvalue corresponds.

A.2 Matrix Method

The coupled second-order The equations of motion can be reduced to a set of second-order differential equations,

$$-\varphi'' + V_1(z)\varphi + f(z)\pi = 0, \tag{A.12}$$

$$-\pi'' + V_2(z)\pi + g(z)\varphi = 0, \tag{A.13}$$

where the eigenvalues are contained within the coefficient functions. These equations can be expressed as a system of first-order differential equations

$$\Phi' + W(z)\Phi = 0, \tag{A.14}$$

where W is the matrix

$$W = \begin{pmatrix} 0 & 1 & 0 & 0 \\ V_1(z) & 0 & f(z) & 0 \\ 0 & 0 & 0 & 1 \\ g(z) & 0 & V_2(z) & 0 \end{pmatrix} \tag{A.15}$$

and Φ is the vector

$$\Phi_{\alpha i} = \begin{pmatrix} \varphi_i \\ -\varphi_i' \\ \pi_i \\ -\pi_i' \end{pmatrix} \tag{A.16}$$

that forms an orthonormal basis of solutions. We can propagate the solution Φ between two boundary points

$$\Phi(z_f) = U(z, z_f, z_0, m_n^2)\Phi(z_0), \tag{A.17}$$

where we solve (A.14) with the appropriate boundary condition at z_0. The eigenvectors and eigenvalues of U are then calculated. Two of the solutions are divergent, but the solutions that correspond to the two smaller eigenvalues do not diverge. We label the non-divergent solutions as the eigenvectors u_3 and u_4. The non-divergent solutions for Φ_i can be written as a linear combination of u_3 and u_4

$$\Phi_i = \alpha u_3 + \beta u_4. \tag{A.18}$$

Non-trivial values of α and β satisfy

$$\begin{pmatrix} u_3^1 & u_4^1 \\ u_3^3 & u_4^3 \end{pmatrix} \begin{pmatrix} \alpha \\ \beta \end{pmatrix} = 0 \tag{A.19}$$

for Dirichlet or

$$\begin{pmatrix} u_3^2 & u_4^2 \\ u_3^4 & u_4^4 \end{pmatrix} \begin{pmatrix} \alpha \\ \beta \end{pmatrix} = 0 \tag{A.20}$$

for Neumann boundary conditions. The values of m_n^2 that minimize the determinant of the matrix (A.19) or (A.20) are the eigenvalues of the system (A.12-A.13). An abrupt change in its behavior of the plot of the determinant vs. the value of m_n signals the location of an eigenvalue.